Influence of Cold-Worked Structure on Electrochemical Properties of Austenitic Stainless Steels

B. RAVI KUMAR, B. MAHATO, and RAGHUVIR SINGH

The effect of cold working on microstructure and structure and thereby on electrochemical behavior of metastable AISI 304L and stable AISI 316L austenitic stainless steels in two different solutions is presented here. The solution-annealed stainless steel (SS) plates were unidirectionally cold rolled at different rolling conditions (with or without interpass cooling and subzero temperature) up to 90 pct reduction in thickness. The X-ray diffraction (XRD) technique was employed to study textures and residual stress development in the stainless steels due to cold working and to quantify the volume fraction of α'-martensite phase formed in the metastable SS. Cold working introduced residual stress and developed texture in both stainless steels. The residual stress and volume fraction of strain-induced α'- martensite phase in 304L SS was varied with the rolling conditions. The study has shown that the type of textures developed in the two stainless steels influenced their electrochemical properties.

DOI: 10.1007/s11661-007-9224-4
© The Minerals, Metals & Materials Society and ASM International 2007

I. INTRODUCTION

BECAUSE austenitic stainless steel (SS) is an fcc lattice structure, it is expected to deform by the movement of dislocations through slip during cold working. However, temperature, strain rate, and strain are the important parameters that can affect the deformation mechanism from slip to twinning and hence the deformation microstructure of austenitic SS.[1–3] Among the material properties, stacking fault energy (SFE) is one of the most important factors for producing changes in the deformation microstructure in austenite SS. Due to the difference in SFE, austenite SS produces a variety of deformation microstructures, such as tangled dislocations, dislocation pileups, stacking faults, and twins.[1,4,5] Further, it is reported that cryogenic deformation produces more stacking faults and twins compared to room-temperature deformation.[2,7] Even high speed[4] or heavy deformation at room temperature[6] found to produce twinned microstructure.

Various metallurgical and processing variables dictate the corrosion resistance of stainless steels.[7] The austenitic grade is considered to be most resistant to industrial atmospheres including aggressive aqueous and nonaqueous acid media. However, as conditions become more severe, addition of several alloying elements is useful in promoting corrosion resistance and hence is desirable. Chromium >12 pct, for instance, improves the passivity of iron alloys, and molybdenum (>2 pct) promotes resistance to pitting corrosion.[8,9] Similarly, sensitization that occurs in stainless steels in the temperature range 500 °C to 870 °C leading to intergranular corrosion can be improved by lowering carbon <0.03 pct or by addition of carbide formers, *e.g.*, titanium and niobium. The degree of susceptibility after heating in this range is a function of time, temperature, and composition.[10] Some grades of SS often behave as metastable alloys in which cold deformation or high-temperature exposure leads to the formation of a second phase and may change corrosion behavior. For example, in a 304 SS variety, the austenite phase transforms to ε or α'-martensite phase either by subzero temperature quenching or by plastic deformation.[11–13] On the other hand, in a 316 SS variety, cold deformation does not lead typically to any significant second-phase formation. The presence of strain-induced α'-martensite phase makes corrosion behavior of stainless steels (such as in 304 SS) even more complex. The α'-martensite that is often introduced by cold working in SS deteriorates their corrosion resistance by selective anodic dissolution.[14] Therefore, the properties of a SS can be affected by a combination of various microstructural features, namely, dislocation density and morphology, grain size and shape, grain boundary substructure, the types of various phases, texture, *etc.*[14]

This article presents the results of electrochemical studies on 304L and 316L SS in sulfuric acid and sodium chloride environments. Solutions were chosen to investigate the effect of cold deformation and subsequent microstructural changes on electrochemical response in the active-to-passive region (in H_2SO_4 solution) and in the passive region/pitting potential (in NaCl solution). In the case of 304L SS, three rolling conditions, namely, cold rolling with cooling between the roll passes (interpass) and without interpass cooling and subzero rolling, were considered with the objective of varying the volume fraction of α'-martensite in the austenite matrix. The studies on 316L SS were restricted to the interpass rolling condition only as no significant phase transformation is expected.

B. RAVI KUMAR, Scientist, and B. MAHATO, Technical Assistant, Materials Science and Technology Division, and RAGHUVIR SINGH, Scientist, Applied Chemistry and Corrosion Division, are with the National Metallurgical Laboratory, Jamshedpur 831 007, India. Contact e-mail: ravik_in@yahoo.com
Manuscript submitted July 4, 2006.
Article published online July 21, 2007.

Table I. Chemical Composition of the 304L and 316L SS

Elements (Wt Pct)	C	Si	Mn	P	S	Cr	Ni	Mo
304L	0.03	0.54	1.8	0.028	0.014	18.55	9.5	—
316L	0.025	0.3	1.2	0.03	0.005	16.90	10.60	2.06

II. EXPERIMENTAL

A. *Materials*

The as-received 304L SS and 316L SS plates (10-mm thick) were solution homogenized at 1080 °C for 1 hour followed by water quenching. Drillings were collected after removing the external oxidized layer and were analyzed for their chemistry. The alloy composition of the two stainless steels is given in Table I.

B. *Materials Processing*

Cold working was performed by multipass unidirectional cold rolling with 10 pct in thickness reduction at each pass in a two-high rolling mill under oil lubrication. Both stainless steels were cold rolled at room temperature to 30, 50, 70, and 90 pct of their original thickness (10 mm) with interpass cooling. However, for 304L SS, cold working was performed without interpass cooling at room temperature and under subzero temperature. Subzero deformation was carried out by quenching the specimen in liquid nitrogen, holding it for 15 minutes at that temperature, and then rolling to 30 pct of thickness reduction. After subzero deformation up to 30 pct, the material was allowed to attain room temperature and further cold rolling was performed to reduction of 50 and 90 pct with interpass cooling.

C. *Microstructural Characterization*

Microstructural examination of the cold-rolled sheets after different reductions was carried out by standard metallographic techniques. A mixture of HCl (3 parts) and HNO_3 (1 part) was used to reveal the microstructure under optical microscopy. Transmission electron microscopy (TEM) studies were carried out on thin foils parallel to the rolling surface using a PHILIPS* CM-200 unit.

*PHILIPS is a trademark of Philips Electronic Instruments Corp., Mahwah, NJ.

The thin foils were prepared by initially polishing mechanically on SiC paper to reduce the starting thickness to 0.5 mm. Finally, TEM foils were prepared by jet polishing in a solution of 95 pct acetic acid and 5 pct perchloric acid bath at a temperature of 12 °C to 14 °C.

The phase transformation studies of α'-martensite in cold-worked 304L SS were performed by the X-ray diffraction (XRD) method by using a K_β filtered Mo K_α radiation on Seifert PTS 3003 XRD (Germany). Autoquan, commercial software based on Rietveld refinement of full pattern, supplied by M/s Seifert (Germany) was used to quantify the volume fractions of martensite.

D. *Residual Stress and Texture Determination*

Residual stress in the austenite and martensite phases of the cold-worked specimens was measured by XRD using the $\sin^2 \Psi$ method[15] and Cr K_α radiation. For this, {220} *hkl* planes of austenite phase and {211} *hkl* planes of martensite were used in the present study. For converting strain measured by XRD, the X-ray elastic constant $(1 + \nu)/E$ was used, where E is Young's modulus and ν is Poisson's ratio. To calculate residual stress, an X-ray elastic constant value of 3.25×10^{-5} $(kg/mm^2)^{-1}$ and 2.62×10^{-5} $(kg/mm^2)^{-1}$[16] was used at small and large deformations, respectively.

The texture was measured by the conventional Schultz reflection technique[17] using a Seifert XRD 3003 PTS diffractometer. Three incomplete pole figures for the (200), (220), and (311) reflections for the austenite phase and (200), (211), and (222) reflections for the martensite phase were recorded using Mo K_α radiation. The experimental pole figure data collected were used to calculate the orientation distribution function (ODF) plots using LaboTex software, developed by LaboSoft s.c. (Poland),[18,19] and presented in the Euler space defined by three Bunge's Euler angles ϕ_1, Φ, and ϕ_2.

E. *Electrochemical Studies*

The anodic polarization measurements were performed on a rolling plane in 1 N sulfuric acid (H_2SO_4) as well as in 0.1 N sodium chloride (NaCl) solutions. The solutions were prepared by adding the requisite amount of analytical reagent grade chemicals to the distilled water. The specimens of size 10×10 mm were mounted on the araldite to expose a 1 cm^2 area to the experimental solution. Samples for polarization study were polished up to 1200-grit emery papers followed by degreasing in acetone solutions, before mounting onto araldite. The rear surface of the specimen was connected to the potentiostat using insulated (by araldite) copper wire. Before polarizing, the specimens were cathodically cleaned at a potential of –900 mV with respect to a saturated calomel electrode for 120 seconds to remove the pre-existing oxides, if any. Scanning was initiated at a potential of –100 mV with respect to the open circuit potential at a scan rate of 6 V/h. It was then reversed (in NaCl solutions) from the transpassive region at the same scan rate. The specimens, after anodic polarization tests, were examined under the optical microscope to ensure that no crevice formation occurs at the interface

of araldite and working electrode. A PARC 273 model potentiostat/galvanostat equipped with corrosion software was used for conducting electrochemical polarization experiments.

III. RESULTS AND DISCUSSION

A. *Microstructure of Cold-Worked Austenitic Stainless Steels*

The starting material revealed polygonal grain features for the two stainless steels, as shown in Figure 1. Cold working resulted in elongation of initial polygonal grain structure along the rolling direction, as depicted in Figure 2. The TEM microstructural study revealed a high dislocation density with some isolated microbands in austenite matrix at smaller thickness reductions. Increasing cold work was found to enhance the dislocation density in the austenite structure and also increase the frequency of microbands in the matrix, as shown by Figure 3. Twinning was also observed along with the formations of α-martensite laths in 304L SS.

The 304L SS, which is stable at room temperature, transforms to martensite during plastic deformation at room or subzero temperature. The martensitic transformation of SS normally leads to formation of two products: one magnetic and bcc (α′) and other, nonmagnetic and hexagonal close-packed (ε).[2,20–37] Results of quantitative phase analysis of the cold-worked 304L SS samples are shown in Table II. Deformation-induced phase transformation was notably lower in the specimens without interpass cooling compared to those with interpass cooling at >70 pct thickness reductions. A low volume fraction of martensite phase in specimens without interpass cooling is due to adiabatic heating of the specimen on subsequent deformation during multipass rolling. This results in higher deformation temperatures with increased rolling and, therefore, inhibited formation of martensite phase. Thus, similar levels of cold working have produced different volume fractions of α′-martensite.

Kinetics of strain-induced martensite formation in 304L SS is well studied by Olson and Cohen,[25] Hecker *et al.*[24,32] and recently by others.[38,39] Hecker *et al.*[24] observed that the austenite $\rightarrow$ α′-martensite transformation can be described by Olson–Cohen analysis in uniaxial tension mode.[25] The volume fraction of α′-martensite phase in this analysis is a sigmoidal function of strain under uniaxial tension loading, and the transformation is very sensitive to temperature in the vicinity of room temperature. The change in volume fraction of α′-martensite obtained in the present study follows the sigmoidal growth at <50 pct reduction where the adiabatic heating is less. Beyond 50 pct reduction, it deviates from sigmoidal growth. Further, the deviation was greater for rolling with interpass cooling. It is also important to mention here that cold rolling deformation used in the present study is not continuous like the uniaxial tension deformation used by Hecker *et al.*[24]

The subzero rolling up to 30 pct thickness reduction led to phase transformations in the 304L SS specimen. Phase quantification showed a volume fraction of 85 pct of α′-martensite in the parent austenite matrix by a mere 30 pct thickness reduction (Table III). Subsequent cold rolling beyond 30 pct was not found to significantly increase the volume fraction of α′-martensite phase.

The results of XRD phase analysis showed identification of only austenite phase in 316L SS under selected processing conditions. Formation of martensitic phase by cold deformation was not expected in 316L SS at room temperature. This is because of the M_{d30} temperature for 316L SS; the temperature at which the martensite forms by deformation is lower than the room temperature.[11]

B. *Residual Stresses*

Residual stress measurements showed different stress trends in the austenite phase of 304L SS and 316L SS with varied percent cold rolling. Results very clearly showed that stresses in the austenite phase decreased with an increase in percent cold rolling. At 90 pct reduction, it is nearly zero in 304L SS, as shown in the Table IV. On the other hand, the martensite phase showed to have increased compressive stresses in two different rolling conditions. Both the rolling conditions showed tensile stresses in austenite phase at <70 pct rolling. The decrease in residual stress for the austenite phase of 304L SS with increasing percent cold rolling may be attributed to strain-induced phase transformation, in

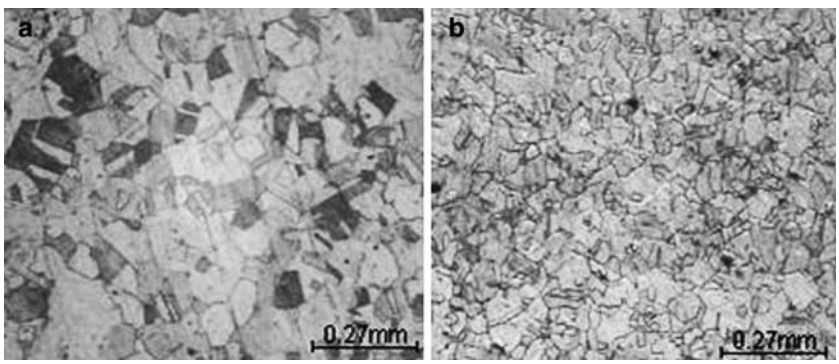

Fig. 1—Microstructures of (*a*) 304L SS and (*b*) 316L SS revealing polygonal grain features after solution anneal treatment.

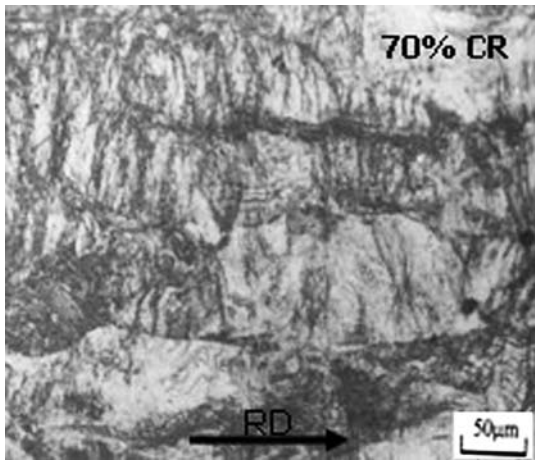

Fig. 2—Microstructures of 70 pct cold-rolled 304L SS showing elongation of initial polygonal grain structure along the rolling direction.

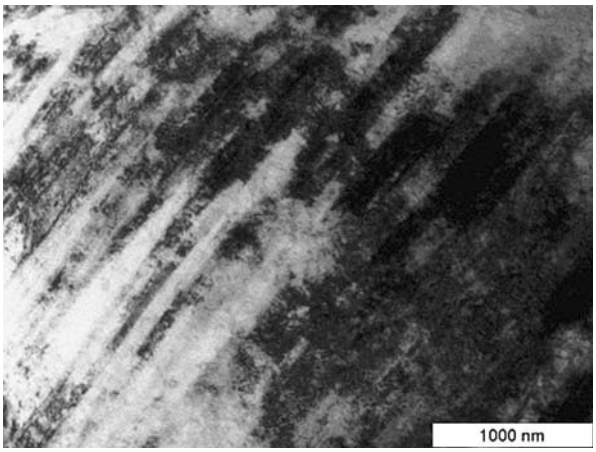

Fig. 3—TEM of 50 pct cold-rolled 304L SS showing dislocation and microband formation.

Table II. Volume Fraction of Martensite Phase during Different Cold Rolling Reductions

Pct CR Reduction	Volume Fraction of α'-Martensite	
	Without Interpass Cooling	With Interpass Cooling
30	10	9
50	25	23
70	34	52
90	56	82

addition to plastic deformation, which results in stress relaxation. Residual stresses in 316L SS containing only the austenite phase showed an increase with percent cold rolling. Similar observations were also reported earlier.[16] The surface preparation procedure for electrochemical studies, which includes mechanical polishing up to 1200 grit SiC paper, was noticed to modify the residual stress of both types of stainless steels and are presented in Table V. The compressive stress of α'-martensite phase was changed to tensile stresses, while the austenite phase

Table III. Volume Fraction of Martensite Phase at Subzero Rolling Temperature

Rolling Condition	Volume Fraction of Martensite Phase
Subzero 30 pct	85
Subzero 30 pct + cold 50 pct rolled	90
Subzero 30 pct + cold 90 pct rolled	92
Subzero 30 pct + cold 90 pct rolled + aged at 500 °C	33
Subzero 30 pct + cold 90 pct rolled + aged at 600 °C	18

continued to remain under tensile stresses below 70 pct reduction and changed to tensile stress at and above it.

C. *Texture of Austenite Phase*

Cold working was expected to introduce texture in both types of SS specimens. The texture is represented by two $<110>$ fibers, namely, α fiber and β fiber, as shown in Figures 4 and 5 for SS cold rolled with interpass cooling. $\{011\}<100>$ Goss (G) to $\{011\}<211>$ Brass (B) as two major texture components were observed in austenite phase at all cold-worked conditions. The other important textural components of fcc alloys, $\{112\}<111>$ Copper (C) and $\{123\}<634>$ S, can be noticed in β fiber plots in Figure 5. Uniform homogeneous β fiber, which includes B, C, and S orientations, was found up to 50 pct reduction for both steels (Figure 5). A maximum in C and S orientations can be observed in the β fiber at 70 pct reduction. This indicates that the material prefers a copper-type texture up to 70 pct cold rolling, and then, on further rolling, it goes through a transition to develop brass-type texture, marked by reduction in the C orientation in β fiber. A similar transition of texture in fcc alloys was reported by Hirsch and Lucke.[40,41] However, in 304L SS without interpass cooling conditions, early maximum of C orientation at 50 pct cold reduction was found. In general, the two stainless steels show similar texture components. The intensities of the texture components for 316L SS were notably lower than for the 304L SS. Further, cold-rolled 304L SS without interpass cooling showed lower ODF intensity for all the texture components compared to those with interpassing cooling condition.

D. *Texture of α'-Martensite Phase in 304L SS*

The volume fraction of α'-martensite was too low to determine texture in 304L SS specimens at cold reduction below 30 pct. Textures at all cold reduction levels are shown using α_{bcc}-fiber and τ-fiber in Figure 6. At 30 pct cold reduction, where the volume fraction of the α'-martensite phase is only 10 pct, the major texture components are $\{113\}<110>$, $\{001\}<110>$, and $\{113\}<211>$ (Figure 6). On increasing the cold reduction to >50 pct, a new component near $\{332\}<113>$ appears. The texture components $\{113\}<110>$ and

Table IV. Residual Stresses in MPa Measured on the As-Rolled Surface Conditions

	304L SS				
	Without Interpass Cooling		With Interpass Cooling		
Pct CR	Austenite	α′-Martensite	Austenite	α′-Martensite	316L SS Austenite
30	145	−54	204	146	33
50	68	−159	163	70	168
70	−85	−485	58	−276	234
90	−7	−300	−7	−450	273

Table V. Residual Stresses in MPa Measured after Surface Prepared for Electrochemical Studies

	304L SS				
	Without Interpass Cooling		With Interpass Cooling		
Pct CR	Austenite	α′-Martensite	Austenite	α′-Martensite	316L SS Austenite
30	134	—	134	—	98
50	151	12	145	29	158
70	141	13	134	49	178
90	136	24	130	53	194

$\{113\}<211>$ formed at 30 pct cold reduction were destabilized at higher deformation and were replaced by $\{112\}<110>$. The $\{112\}<110>$, $\{001\}<110>$, and $\{332\}<113>$ texture components are the main orientations of martensite at all percent of cold rolling, which are well-known components of the bcc cold rolling textures. However, the $\{332\}<113>$ component at larger deformations (> 70 pct) rotates toward the more stable $\{111\}<112>$ orientation as observed at 90 pct cold reduction. The specimens rolled at subzero temperature showed a notable sharp $\{001\}<110>$ texture component. This could be due to the incremental increase in volume fraction of the α′-martensite phase during room-temperature cold rolling and subsequent progressive acquisition of preferred orientation. On the other hand, owing to its larger volume fraction at subzero temperature-deformed condition, it starts acquiring preferred orientation from the beginning of the cold rolling and resulted in sharper $\{001\}<110>$ texture component.

E. *Electrochemical Behavior in 1N H_2SO_4 Solution*

Figure 7 shows the representative electrochemical polarization curves for 304L and 316L SS in 1 N H_2SO_4 solution for different percents of cold working conditions. The material showed active-passive behavior with distinct passivation and prepassive regions for the two stainless steels. It may be seen from Tables VI through VII that the corrosion potential (E_{corr}) became more active with the percent of cold reduction, whereas the primary passive potential (E_{pp}) remained more or less the same (Table VI). The passive current (I_p) is found to increase up to 50 pct cold reduction and then to decrease (Table VI). On the other hand, a very high value of primary passive current (I_{pp}) was noticed at 70 pct of cold reduction without interpass cooling for 304L SS. These findings indicate the effect of cold working on the oxide film behavior.[42,43] Subzero rolling to 30 pct, where a very large volume fraction of martensite formation occurs, did not seem to bring about significant change in the electrochemical response of 304L SS. The prepassive currents of 304L SS were much higher than that of the 316L SS, while the passive currents were of the same order. The lower E_{pp}, I_p, and I_{pp} values for 316L SS than for 304L SS indicate the formation of quicker and more protective film in 316L SS.

F. *Effect of Microstructural Changes in 1 N H_2SO_4 Acid Solution*

The initial increase of passive current in the two stainless steels may be attributable to the development of residual tensile stresses (Table V) and formation of α′-martensite in 304L SS. However, it may be noted that the influence of α′-martensite was observed to be insignificant, as indicated by results on the subzero rolled specimens. The passive current increased with cold work up to 50 pct and decreased then with further rolling (Table VI). Development of sharp crystallographic texture in austenite as well as in α′-martensite phase was found to occur at high cold reduction levels compared to that at low deformation. The phases showed rolling plane crystallographic texture of {011} in austenite and {111}, {112}, and {001} in α′-martensite phases. It has been reported earlier that high density close-packed crystal planes offer high resistance to chemical attack by improving passivation and repassivation behavior.[44] In the present study, high packing

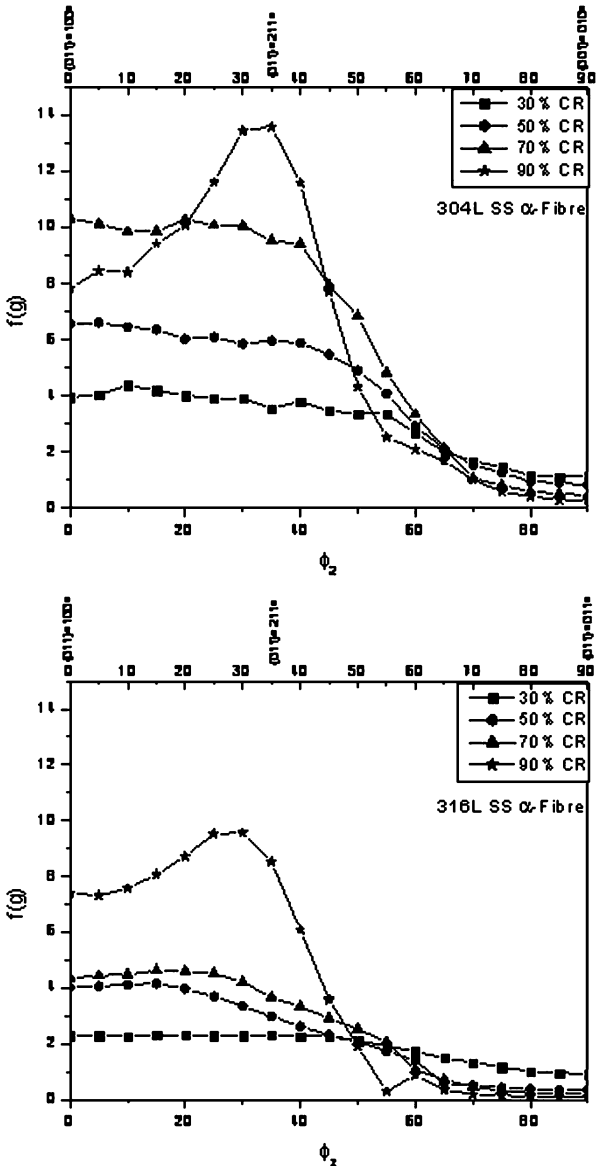

Fig. 4—Orientation density variation in α-fiber for the two stainless steels at different percents of cold rolling with interpass cooling.

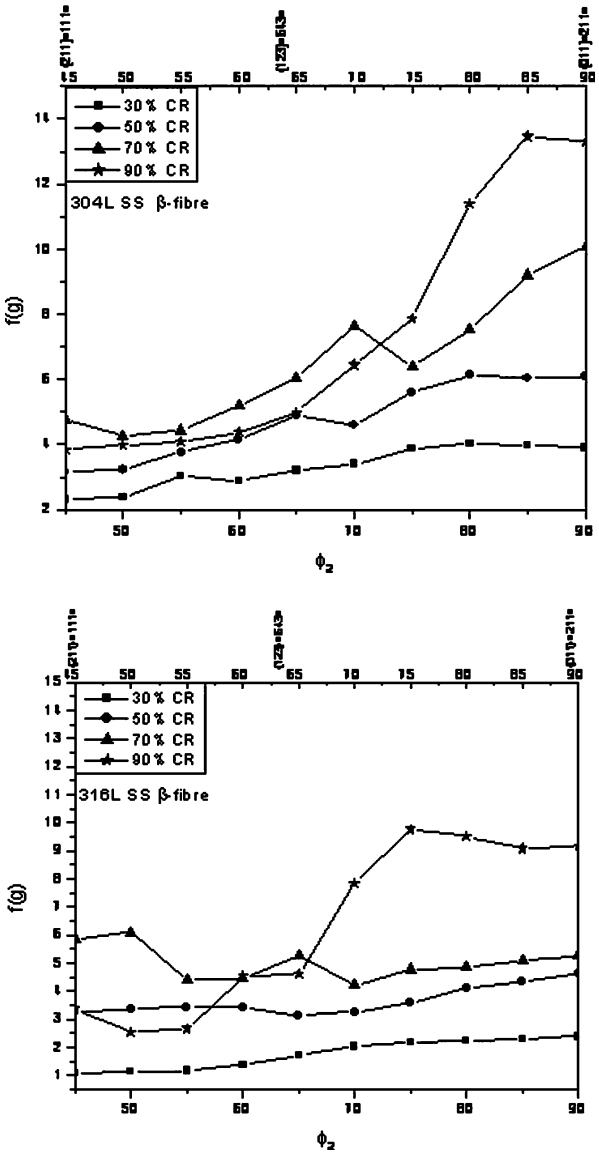

Fig. 5—Orientation density variation along β-fiber for the two stainless steels at different percents of cold rolling with interpass cooling.

density crystal faces of the type {110} in austenite (fcc) phase and {100} as well as {111} in α′-martensite (bcc) phase were observed. These orientations seem to have improved upon passivation properties and nullified the adverse effect of tensile residual stresses at higher deformations. Hence, it may be concluded that the adverse effect of tensile residual stress at higher reductions does not play a dominant role in altering the corrosion kinetics during passivation in sulfuric acid solutions. This is contrary to the earlier studies[42,45] on the role of residual stresses as a result of cold rolling on passivation of 304L SS.

Further, the room-temperature rolling of 304L SS to > 50 pct with interpass cooling reduced the passive current to 0.0140 mA/cm^2, and subzero temperature rolling to 90 pct reduced I_p to 0.014 mA/cm^2. Both rolling reductions showed very high volume fractions of α′-martensite phase with very sharp textures. Correlating this trend with the induced volume fraction of α′-martensite and texture therein, it appeared that the development of sharp textures influences corrosion kinetics during passivation in sulfuric acid solution at higher reductions.

G. *Electrochemical Behavior in 0.1 N NaCl Solution*

Typical electrochemical polarization curves obtained for 304L and 316L SS in 0.1 N NaCl are shown in Figure 8. The pitting potential, E_{pit}, of SS determined in 0.1 N NaCl solution is plotted against percent cold deformation in Figure 9. Cold rolling up to 70 pct was found to reduce the pitting potential; however, it

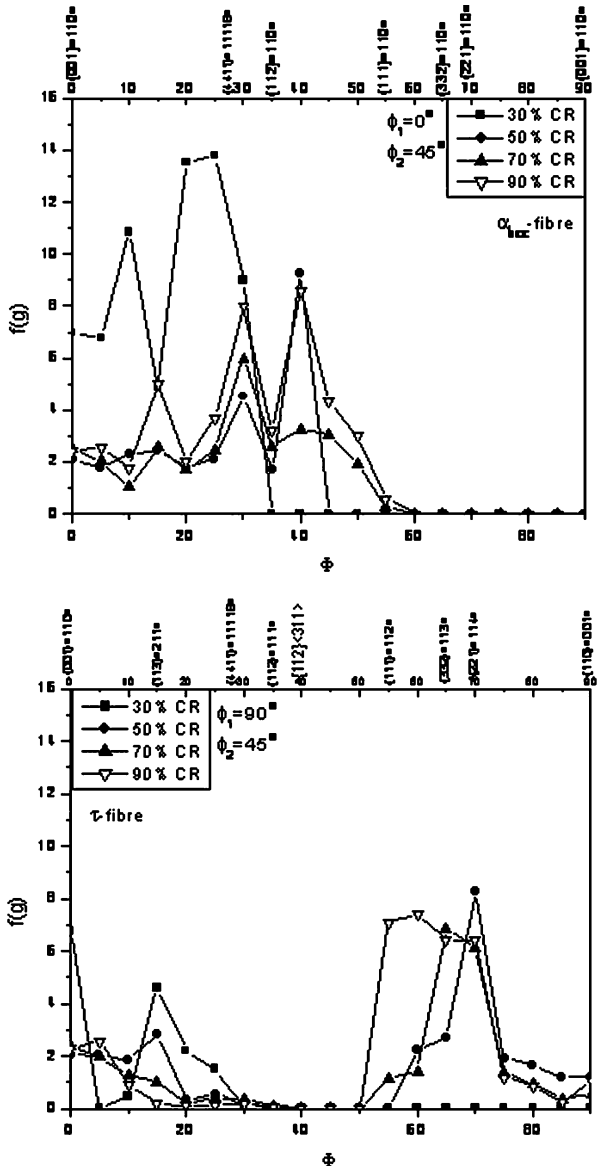

Fig. 6—Orientation density variation along α_{bcc}-fiber and τ-fiber at different percent cold rolling with interpass cooling for α'-martensite phase.

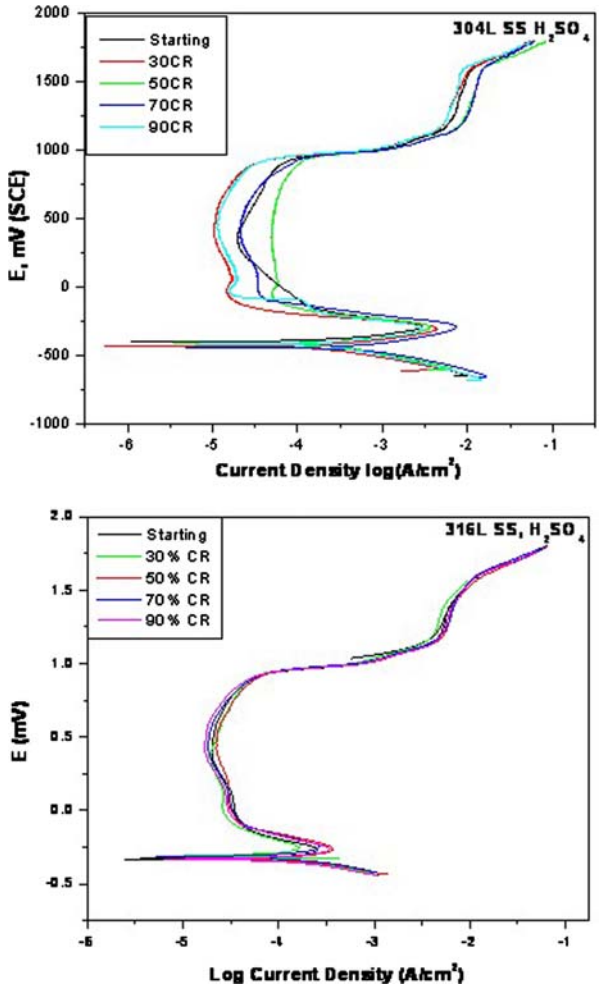

Fig. 7—Electrochemical polarization curves of 304L and 316L SS 1N H_2SO_4 in solution cold rolled with interpass cooling.

increased on further rolling up to 90 pct (Figure 9). Figure 9(a) also showed the variation in pitting susceptibility of specimens subjected to subzero rolling with subsequent higher cold reductions. The trend in pitting susceptibility was similar for all rolling modes of 304L and 316L. Such changes in pitting potentials with the increase in cold work have also been studied by several researchers.[46–50] It was observed that the nature and extent of variations were widely scattered.[46–49] This may be due to the difference in method, *e.g.*, potentiostatic scratch tests,[48,51] anodic polarization,[46,48–50] and pit propagation rate,[46] used for evaluating pitting resistance. The pitting potentials may also vary with

Table VI. Electrochemical Parameters of 304L SS as a Function of Percent Cold Rolling in 1 N H_2SO_4 Solution for Cold Rolling without Interpass Cooling (No IP) and with Interpass (IP)

	E_{corr}, mV		E_{pp}, mV		I_p, mA/cm^2		I_{pp}, mA/cm^2	
Pct CR	No IP	IP	No IP	IP	No IP	IP	No IP	IP
0	−398	−398	−298	−298	0.0163	0.0163	2.97	2.97
30	−414	−414	−301	−301	0.0358	0.0358	3.21	3.21
50	−411	−415	−294	−299	0.0472	0.0438	3.59	3.35
70	−442	−413	−293	−309	0.0187	0.0137	7.30	2.79
90	−414	−420	−289	−302	0.0183	0.0140	5.23	5.47

Table VII. Electrochemical Parameters of 316L SS as a Function of Percent Cold Rolling in 1 N H_2SO_4 Solution

Pct CR	E_{corr}, mV	E_{pp}, mV	I_p, mA/cm^2	I_{pp}, mA/cm^2
0	−330	−251	0.020	0.0240
30	−304	−235.4	0.020	0.015102
50	−327	−244	0.02206	0.034704
70	−315	−227	0.01805	0.024202
90	−330	−247.5	0.017	0.0317

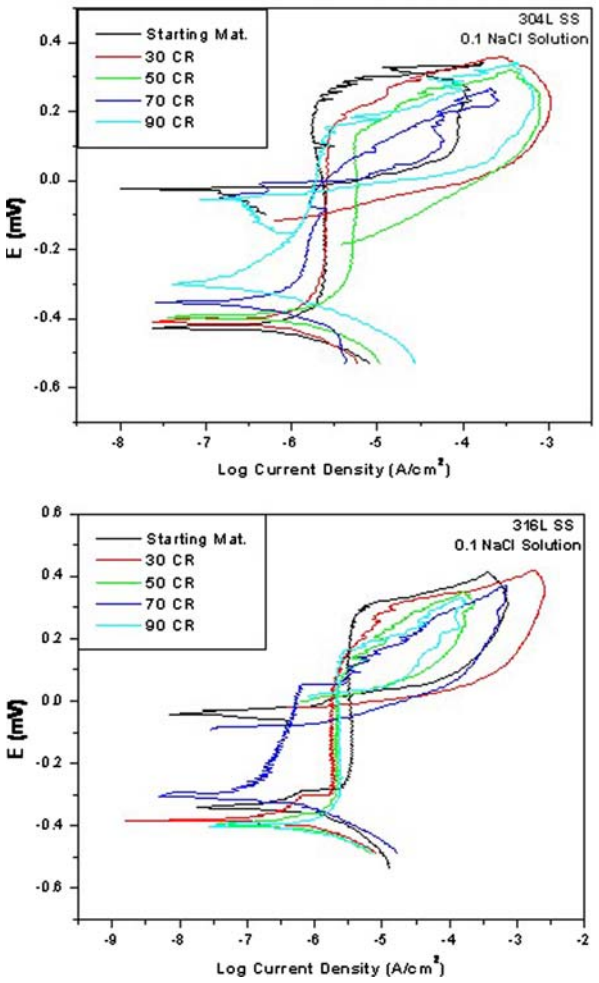

Fig. 8—Electrochemical polarization curves of 304L and 316L SS in 0.1 N NaCl solution.

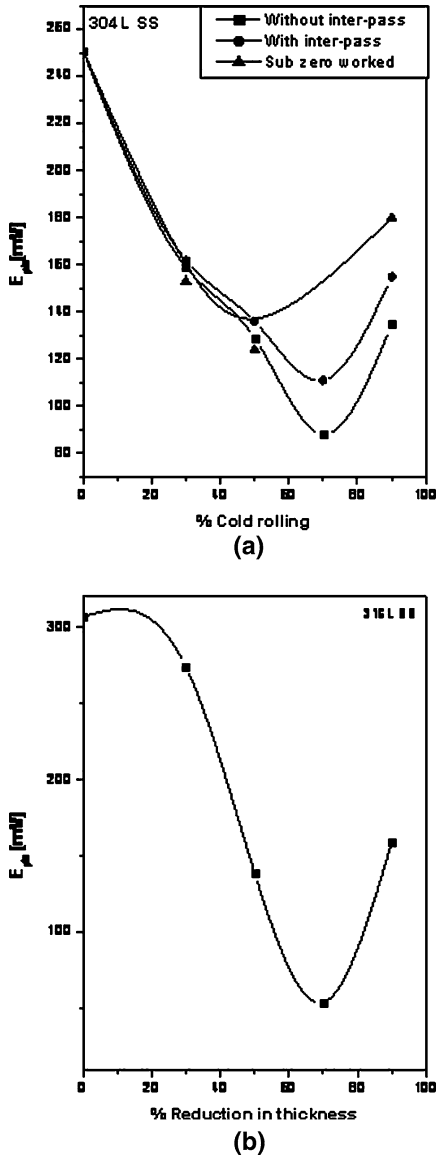

Fig. 9—Variation of pitting potential with percent cold reduction in 0.1 N NaCl solution for 304L and 316L SS.

experimental parameters such as type and concentration of solutions, temperature, pH, *etc.*[49,50] and the extent of deformation applied to materials.

H. *Effect of Microstructural Changes in 0.1 N NaCl Solution*

The changes in pitting potential, in cold-deformed steel or iron, have been reportedly attributed to the stress, deformation-induced α'-martensite, or dislocations. In the present study, the pitting potential, E_{pit}, was found to decrease for cold reductions up to 70 pct and increased thereafter. Similar behavior has also been reported earlier for deformation up to 50 pct.[47,48,50] Others showed contradiction with these findings.[46,49] A monotonous change in pitting potential showed by a few researchers has been attributed to an increase in the pct of α'-martensite.[48,51–53] They, however, used maximum deformation up to 50 pct and reported an increase in percent α'-martensite with percent cold work in 304L SS. In the present study, the stainless steels were deformed to a much higher level, *e.g.*, 90 pct, during which the variation of pitting potentials was found to follow the nonuniform trend with percent of rolling, as illustrated in Figures 9(a) and (b). The variation in pitting potential due to cold deformation from 0 to 90 pct does not appear to have a direct correlation with an increase in the pct α'- martensite. This could be confirmed from the fact that the specimen rolled at subzero temperature had much higher α'-martensite phase (85 pct) compared to

those rolled at room temperature with and without interpass cooling, but showed comparable pitting potential (from 159 to 153 mV). Therefore, the effect of α'-martensite is not expected to cause significant changes in E_{pit}. The change in the pitting potential of 304L SS in the present study may be explained due to either effect of stresses, crystallographic texture, or a combination thereof. The decrease in pitting potential at low (at and below 70 pct) deformations possibly resulted from the residual tensile stresses, as they are known to reduce corrosion resistance.[54] The effect of texture at low deformations appears to be insignificant and only becomes prominent at higher deformations. Texture plays an important role in enhancing Cr diffusion in Fe-Cr alloys.[55] Moreover, a recent[56] study showed that the passive film formed on highly deformed (~66 pct) 304L SS contains a higher Cr/Fe ratio than that in the film on an annealed material. This was attributed to higher pitting potential for the deformed material. Others have also observed that the Cr diffusion is accelerated by cold rolling, which then affects the passivation behavior of austenitic stainless steels.[57,58] Stainless steel cold worked beyond 70 pct in this study has high density close-packed planes and seems to have favored the formation of Cr-rich passive film that increased the pitting potential.

Subzero temperature rolling and subsequent room-temperature rolling were found to produce a similar trend as that of cold deformation at room temperature, as discussed previously. The subzero rolled 304L SS having 85 pct of α'-martensite phase displayed a similar pitting potential as the specimen cold rolled to 30 pct irrespective of the austenitic or martensitic phases present. Cold rolling to 90 pct resulted in the increase of the pitting potential of the material, in spite of containing high tensile residual stress (168 MPa) showing the influence of texture on the pitting potential.

IV. CONCLUSIONS

At low deformations, where cold rolling textures are weak, residual tensile stresses were found to deteriorate electrochemical behavior for both stainless steels, as indicated by the increase in passive current (in H_2SO_4 solutions) and decrease in pitting potential (in NaCl solutions). At deformation levels >70 pct, the pitting resistance was increased as the cold rolling textures became prominent and negated the adverse effect of the tensile residual stresses. The subzero temperature rolled 304L SS, after a drop in pitting potential at levels of cold work, showed the highest recovery (more than 70 pct) of pitting resistance. The 90 pct cold reduction of 304L SS transformed above 80 pct of austenite phase to α'-martensite, and at subzero temperature and cold rolling, nearly 90 pct of austenite changed to α'-martensite. The difference in volume fraction of α'-martensite in the two rolling situations, though, was not significant, but the recovery of the pitting potential was nearly 10 pct more for subzero-rolled SS. In terms of texture, stainless steels cold rolled at subzero temperature revealed very pronounced {001} rolling plane texture compared to that at room temperature. Therefore, the {001} plane, which is the second closest packed plane after the {101} plane for bcc lattice, may be responsible for the maximum recovery in pitting resistance after deterioration at initial rolling levels in 304L SS. On the other hand, lower recovery in the 316L SS than in 304L SS could be due to development of {110} rolling plane texture, which is the third closest packed plane after the {111} and {100} plane of the fcc lattice. Hence, the type of textures developed in the two stainless steels has a strong influence on electrochemical properties in addition to residual stresses.

ACKNOWLEDGMENTS

The authors are grateful to Professor S.P. Mehrotra, Director, National Metallurgical Laboratory, for supporting this work. The authors also record their thanks to Sri P.K. De for helping with cold rolling. The authors record their gratitude to the M/s Salem Steel Plant, Salem, India, for providing the material for the present study.

REFERENCES

1. R.W. Hertzborg: *Deformation, Fracture Mechanics of Engineering Materials*, John Wiley & Sons Inc, New York, NY, 1989.
2. J.W. Brooks, M.H. Loretto, and R.E. Smallman: *Acta Metall.*, 1997, vol. 27, pp. 1829–38.
3. D. Goodchild, W.T. Roberts, and D.V. Wilson: *Acta Metall.*, 1970, vol. 18, pp. 1137–45.
4. M.A. Meyers and K.K. Chawla: *Mechanical Behaviour of Materials*, Prentice-Hall, Inc., Englewood Cliffs, New Jersey, 1998.
5. L.E. Murr: *Interfacial Phenomena in Metals and Alloys*, Addison-Wesley, New York, 1975.
6. P. Mullner and C. Solenthaler: *Mater. Sci. Eng. A*, 1997, vol. 230, pp. 107–15.
7. F.B. Pickering: *Int. Mater. Rev.*, 1976, vol. 21, pp. 227–68.
8. R.J. Brigham and W.J. Tozer: *Corrosion*, 1974, vol. 30, pp. 161–66.
9. M.A. Streicher: *Corrosion*, 1974, vol. 30, pp. 77–91.
10. L.Y.A. Seukins and E.G. Fel'dgandler: *Metalloved. Term. Obra Met.*, 1968, vol. 11, pp. 10–13.
11. A. Tryggve: *J. Iron Steel Inst.*, 1954, vol. 177, pp. 165–74.
12. R.P. Reed: *Acta Metall.*, 1962, vol. 10, pp. 865–77.
13. R. Langneborg: *Acta Metall.*, 1964, vol. 12, pp. 823–43.
14. P. Marshal: *Austenitic Stainless Steel: Microstructure and Mechanical Properties*, Elsevier, London, 1984.
15. I.C. Noyan and J.B. Cohen: *Residual Stress Measurement by X-ray Diffraction and Interpretation*, Springer Verlag, New York, NY, 1987.
16. A. Bahadur, B. Ravi Kumar, and S. Ghosh Chowdhury: *Mater. Sci. Technol.*, 2004, vol. 20, pp. 387–92.
17. L.G. Schulz: *J. Appl. Phys.*, 1949, vol. 20, pp. 1030–33.
18. K. Pawlik and P. Ozga: *LaboTex: The Texture Analysis Software*, Göttinger Arbeiten zur Geologie und Paläontologie, SB4, 1999.
19. K. Pawlik: *Phys. Staus Solidi B*, 1986, vol. 134, pp. 477–83.
20. A.H. Eichelman and F.C. Hull: *J. Trans ASM*, 1953, vol. 45, pp. 77–104.
21. P.L. Manganon, Jr. and G. Thomas: *Metall. Trans.*, 1970, vol. 1, pp. 1577–86.
22. P.L. Manganon, Jr. and G. Thomas: *Metall. Trans.*, 1970, vol. 1, pp. 1587–94.
23. G.B. Olson and M. Cohen: *J. Less-Common Met.*, 1972, vol. 28, pp. 107–18.
24. S.S. Hecker, M.G. Stout, K.P. Staudhammer, and J.L. Smith: *Metall. Trans. A*, 1982, vol. 13A, pp. 619–26.

25. G.B. Olson and M. Cohen: *Metall. Trans. A*, 1975, vol. 6A, pp. 791–95.
26. P.C. Maxwell, A. Goldberg, and J.C. Shyne: *Metall. Trans.*, 1974, vol. 5, pp. 1305–17.
27. F. Lecroisey and A. Pineau: *Metall. Trans.*, 1972, vol. 3, pp. 387–96.
28. R.P. Reed: *Acta Metall.*, 1962, vol. 10, pp. 865–77.
29. B. Cina: *JISI*, 1954, vol. 177, pp. 406–22.
30. J.A. Venables: *Phil Mag.*, 1962, vol. 7, pp. 35–44.
31. J. Dash and H.M. Otte: *Acta Metall.*, 1963, vol. 11, pp. 1169–78.
32. L.E. Murr, K.P. Staudhammer, and S.S. Hecker: *Metall. Trans. A*, 1982, vol. 13A, pp. 627–35.
33. T. Suzuki, H. Kojima, K. Suzuki, T. Hashimoto, and M. Ichihara: *Acta Metall.*, 1977, vol. 25, pp. 1151–62.
34. J.R. Patel and M. Cohen: *Acta Metall.*, 1953, vol. 1, pp. 531–38.
35. H.M. Otte: *Acta Metall.*, 1957, vol. 5, pp. 614–27.
36. M.W. Bowkett, S.R. Keown, and D.R. Harries: *Met. Sci.*, 1982, vol. 16, pp. 499–517.
37. K. Takashima, Y. Higo, and S. Numomura: *Phil. Mag.*, 1984, vol. 49 A, pp. 231–41.
38. H.C. Shin, T.K. Ha, and Y.W. Chang: *Scripta Mater.*, 2001, vol. 45, pp. 823–29.
39. Z. Tourki, H. Bargui, and H. Sidhom: *J. Mater. Proc. Technol.*, 2005, vol. 166, pp. 330–36.
40. J. Hirsch and K. Lucke: *Acta Metall.*, 1988, vol. 36, pp. 2863–82.
41. J. Hirsch and K. Lucke: *Acta Metall.*, 1988, vol. 36, pp. 2883–904.
42. Z.A. Foroulis and H.H. Uhlig: *J. Electrochem. Soc.*, 1964, vol. 111, pp. 522–28.
43. A. Barbucci, M. Delucchi, M. Panizza, M. Sacco, and G. Cerisola: *J. Alloys Compounds*, 2001, vol. 317, pp. 607–11.
44. S.S. Chouthai and K. Elayaperumal: *J. Br. Corr.*, 1976, vol. 11, pp. 40–43.
45. U.R. Evans: *Corrosion and Oxidation of Metals*, Edward Arnold Ltd, London, 1960, pp. 386–89.
46. B.C. Syrett and S.S. Wing: *Corrosion*, 1978, vol. 34, pp. 138–45.
47. C.J. Semino, P. Pedeferri, G. Burstein, and T.P. Hoar: *Corr. Sci.*, 1979, vol. 19, pp. 1069–78.
48. J.C. Rowlands: *Br. Corr. J.*, 1976, vol. 11, pp. 195–98.
49. U.K. Mudali, P. Shankar, S. Ningshen, R.K. Dayal, H.S. Khatak, and Baldev Raj: *Corr. Sci.*, 2002, vol. 44, pp. 2183–98.
50. U.K. Mudali, S. Ningshen, A.K. Tyagi, and R.K. Dayal: *Mater. Sci. Forum*, 1999, vols. 318–320, pp. 495–502.
51. B. Mazza, P. Pedeferri, D. Sinigaglia, A. Liganda, G.A. Mandora, G. Re, G. Taccani, and D. Wenger: *J. Electrochem. Soc.*, 1979, vol. 126, pp. 2075–89.
52. A. Cigada, G. Rondelli, and B. Vicentini: *Proc. Int. Conf. Martensitic Transformation*, The Japan Institute of Metals, Sendai, Japan, 1986, pp. 527–32.
53. C. Eckstein, A. Welss, D. Janke, and D. Peisker: *Proc. Int. Congr. Stainless Steels 99, Science and Market*, Chia Laguna Sardinia, Italy, June 6–9, 1999, Associaziona Italiana di Metallurgia, Italy, 1999, pp. 34–36.
54. H.E. Hanninen: *Int. Mater. Rev.*, 1979, vol. 3, pp. 85–135.
55. C.L. McBee and J. Krugher: *Electrochim. Acta*, 1972, vol. 17, pp. 1337–41.
56. S.V. Phadnis, A.K. Satpati, K.P. Muthe, J.C. Vyas, and Sundareshan: *Corr. Sci.*, 2003, vol. 45, pp. 2467–83 .
57. A. Barbucci, G. Cerisola, and P.L. Carbot: *J. Electrochem. Soc.*, 2002, vol. 149, pp. 534–42.
58. R. Singh, B. Ravi Kumar, A. Kumar, P.K. Dey, and I. Chattoraj: *Metall. Mater. Trans. A*, 2003, vol. 34A, pp. 2441–47.